

Improvement of surface morphology of thin films and performance by “electrical annealing” on polymer solar cells

Meng Li,^{1,2} Heng Ma,^{1,2, a)} Xiu Gong,^{1,2} Lulu Jiang,^{1,2} Heying Niu,¹ and Adil Amat¹

¹⁾Department of Physics, Henan Normal University, Xinxiang 453007, China

²⁾Henan Key Laboratory of Photovoltaic Materials, Xinxiang, 453007, China

An external electric field (EEF) is applied on the film, which is spin coated with poly (3-hexylthiophene): [6,6]-phenyl C₆₁ butyric acid methyl ester (P3HT: PCBM) during its annealing process, to improve the performances of bulk heterojunction polymer solar cells (PSCs). This treatment can orientate the molecular order of the polymer materials and change the morphology of the active layer. The experimental results show that the EEFs can cause the surface of the active film to become needle morphology, and make the root mean square roughness of active layer increase. With the different EEFs during the active layer annealing, the short circuit current density of PSC is improved from 5.55 mA/cm² to 6.75 mA/cm², the power conversion efficiency increases from 1.05% to 1.31%, and the incident photon-to-current conversion efficiency increases from 44% to 49%, respectively. As a conclusion, EEF treatment can effectively improve the surface morphology and increase the area of the active layer which can reduce the contact resistance, therefore, is beneficial to enhance the mobility of charge carriers formed inside the active layer of PSC.

1. INTRODUCTION

Polymer solar cells (PSCs) have attracted considerable attention due to their light weight, mechanical flexibility, low production cost, and the large area manufacturing approach¹⁻⁴. Recently, PSCs with power conversion efficiency (PCE) of 6-8% have been achieved based on the conventional device architecture using the advanced conjugated polymers as donors and fullerene derivatives as acceptors⁵⁻⁸. However, still much lower PCE and poorer stability and lifetime than Si-based solar cells limits the industrialization of PSCs. Therefore, further improvement in the device performance of PSCs is necessary.

The most commonly investigated PSCs processed from solution are the conjugated polymers poly-3(hexylthiophene) (P3HT) serving as donor and [6, 6]-phenyl-C₆₁-butyric acid methyl ester (PCBM) as acceptor⁹⁻¹¹. Many approaches, such as thermal annealing, solvent annealing and adding additives, have been used to improve the performance of P3HT: PCBM system¹²⁻¹⁵. These processes mainly focus on the further increase of the molecular crystallinity, improve the orderliness of the molecular arrangement and optimize the morphology of active layer¹⁶⁻¹⁸; ultimately, these approaches are capable of enhancing the carrier mobility and improving charge transport. However, these approaches can not avoid the active layer materials, especially for PCBM, to aggregate effectively, which leads to a nonuniform and disorder of bulk heterojunction to influence the carrier mobility and charge transport¹⁹. This is the key factor to result in the poor stability and lower PCE of PSCs.

In order to optimize the morphology of active layer and reduce PCBM aggregation, some studies have applied an electric field on PSC devices²⁰⁻²². Ma et al.²³ reported that they have applied a voltage on metal plates outside

the device to build a smaller external electric field (EEF) (about 10⁵ V/m) during the drying process. This work considered the polar effects of internal molecules in the active layer under the applied EEF, but maybe they did not get the most optimal effect in the process. Because thermal annealing can make the phase separation of the active layer reach a better condition, meanwhile the internal molecules are active and restless, to apply an EEF on active layer during the annealing process maybe can effectively improve the uniform and order in forming the bulk heterojunction. In this study, different EEFs were applied during the active layer annealing process; the influence of this treatment on PSCs performance was more precisely investigated based on molecular crystallize and morphology characterization of the active layer.

2. EXPERIMENT

2.1 Experimental materials

A pre-patterned indium tin oxide (ITO) glass with a sheet resistance of average 15 Ω/□ and transmission 85% was purchased from Kaivo. Regioregular active materials P3HT and PCBM were purchased from Luminescence Technology Corp. and Solenne BV. As an aqueous dispersion, Poly (3, 4-ethylenedioxythiophene): poly (4-styrenesulfonate) (PEDOT: PSS) (AI 4083) was purchased from Bayer AG. All the chemicals were used as received without further purification.

2.2 Device fabrication and characterization

The structure of the device, Glass / ITO / PEDOT:PSS (50nm) / P3HT: PCBM (180nm) / Al (100nm), employed in this study is shown in Fig.1(a). In the period of active layer annealing, different vertical EEFs were exerted on the blended layer of P3HT:PCBM.

^{a)}Electronic mail:hengma@henannu.edu.cn.

The diagram of the device exerted the electric field is shown in Fig.1(b). The vertical EEF treatments were divided into two conditions according to the direction of the electric field: up (+) and down (-) electric field.

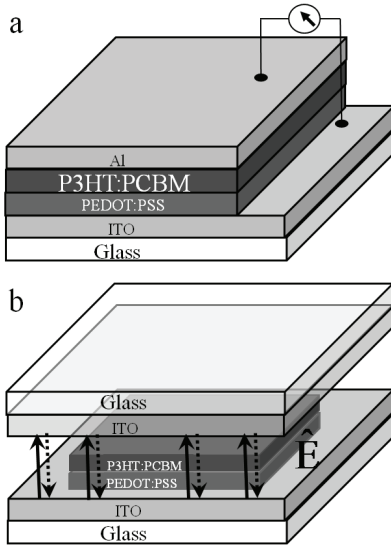


FIG. 1. Schematic structure of (a) devices and (b) vertical electric field treatment (the solid line is a symbol for up (+) direction, and the dashed line is a symbol for down (-) direction.)

All of the production processes adopted in this work are listed as follow.

Substrates cleaning: aqueous detergent / acetone / alcohol / deionized water (15 min each process, at 30°C, in ultrasonic basin). The cleaned substrates were dried in air.

PEDOT: PSS spin coating (thickness: 50 nm): 1500 rpm 15 s / 3000 rpm 45 s / 110°C annealed 30 min (in air).

Preparation of active layer solution: P3HT 10 mg, PCBM 9 mg, 1, 2-dichlorobenzene 1 mL are mixed and stirred at 50°C for 24 h.

Spin coating of active layer (thickness 180 nm): 700 rpm 1 min / 110°C annealed 10 min (in air).

DC power supply (Capacitance value): DC 30V ($\pm 0.4 \times 10^6$ V/m), 60V ($\pm 0.8 \times 10^6$ V/m) (Agilent E3649A); 90V ($\pm 1.3 \times 10^6$ V/m), 120V ($\pm 1.7 \times 10^6$ V/m), 150V ($\pm 2.1 \times 10^6$ V/m) (SS1712 Shijiazhuang City Radio Factory).

Al electrode evaporation (thickness 100 nm): Purity 99.995% / Vacuum degree 5×10^{-4} Pa / deposition rate 0.9 nm/s.

Solar simulator: 1000 W Xenon lamp simulator source AM 1.5 G, 100 mW/cm² (Abet Technologies Cop.).

Current density voltage (J-V) curves measurement: four wires method, Keithley 2400 source meter.

Atomic force microscopy (AFM) measurement: tapping mode (Veeco NanoScope 3D).

Incident photon-to-current conversion efficiency

(IPCE) measurement: 1000 W halogen lamp, grating monochromator (Acton Spectra Pro 2300i).

The IPCE for a certain wavelength λ was expressed as:

$$\text{IPCE} = \frac{1240 \times J_{sc}}{\lambda \times P_{in}}, \quad (1)$$

Where J_{sc} is the short circuit current density in A/cm², λ is the wavelength in nm, and P_{in} is the monochromatic light incidence in W/m².

3. RESULTS AND DISCUSSION

The measured J-V characteristic of the devices with different EEF treatments under white light illumination at intensity of 100 mW/cm² is shown in Fig. 2; and the corresponding data including PCE, FF, series resistor (R_s) and shunt resistor (R_{sh}) are listed in Table I. The open symbol expresses the up EEF, and the solid symbol describes the down EEF, which the EEF direction is defined in Fig. 1 (b). In a comparison of the device with up and down EEF treatments, the obvious difference in the data of the short-circuit current density (J_{sc}) is interesting. Compared with no EEF treatment, the EEFs with down direction result in a marked increase of J_{sc} , furthermore, J_{sc} increases successively as the down EEF increases. On the conversely, the up EEF brings a slight decrease of J_{sc} compared with no EEF treatment. However, the changes of J_{sc} with different up EEFs are small. From Table 1, the difference of J_{sc} between the largest down EEF (2.1×10^6 V/m) and the largest up one reaches 1.6 mA/cm².

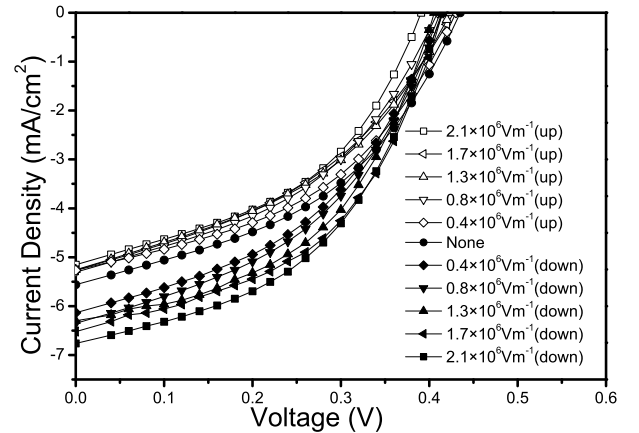


FIG. 2. J-V characteristics of the PSC devices with different vertical electric field treatments under 100 mW/cm² AM 1.5 G irradiation. The open symbol expresses the up electric field, and the solid symbol describes the down electric field, which the electric field direction is defined in Figure 1 (b).

For the open circuit voltage (V_{oc}), one can find that the differences of V_{oc} are un conspicuous with different EEFs no matter for up or down direction. Just like V_{oc} , the fill factors (FF) of all the devices are barely changed for the different EEFs.

TABLE I. The performance of P3HT: PCBM PSCs under different vertical electric field treatments.

External electric field (Vm^{-1})	J_{sc} (mA/cm^2)	V_{oc} (V)	FF	PCE(%)	R_s (Ω)	R_{sh} (Ω)
2.1×10^6 V/m (down)	6.75	0.41	0.47	1.31	571	4881
1.7×10^6 V/m (down)	6.53	0.41	0.48	1.30	589	4672
1.3×10^6 V/m (down)	5.30	0.40	0.47	1.22	583	6141
0.8×10^6 V/m (down)	6.35	0.41	0.43	1.15	697	4351
0.4×10^6 V/m (down)	6.13	0.41	0.43	1.11	752	4638
0 V/m	5.55	0.43	0.43	1.05	877	4846
0.4×10^6 V/m (up)	5.25	0.43	0.44	1.00	886	5573
0.8×10^6 V/m (up)	5.30	0.40	0.42	0.93	888	4600
1.3×10^6 V/m (up)	5.26	0.42	0.41	0.91	943	4364
1.7×10^6 V/m (up)	5.26	0.42	0.40	0.90	1045	4470
2.1×10^6 V/m (up)	5.15	0.39	0.44	0.89	794	4666

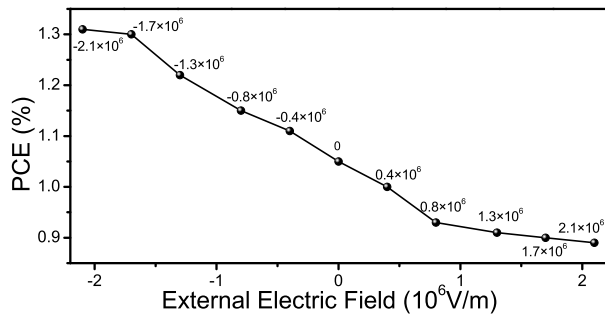


FIG. 3. The dependence of PCE of PSCs is plotted as a function of different vertical electric fields.

Figure 3 shows PCE of PSCs as a function of different vertical EEFs divided up and down direction. It is obvious that the changes of PCE of the devices are different with the direction of the EEF compared to no field. For the down EEF, PCE of the devices increases with the increasing EEF intensity almost in line relationship until the EEF is equal to a value of 1.7×10^6 V/m (D.V. 120 V). Increasing the EEF intensity to 2.1×10^6 V/m, the increase of PCE becomes slowly and the increase trend breaks away from linear relationship. On the other hand, for the up EEFs, PCE of the devices decreases obviously with increasing the EEF intensity in nonlinear correlation. When the EEF intensity exceed 0.8×10^6 V/m (D.V. 60V), PCE of the devices decreased slowly with increasing the EEF intensity. Because the EEF intensity of 2.1×10^6 V/m approaches the breakdown field strength, it seems that PCE also tends to a saturated value both in up and down direction. From 1.05% (no EEF) increased to 1.31% (-2.1×10^6 V/m), maximum 24% increase in PCE with the down EEF was obtained compared with no EEF added. On the contrary, with the up EEF, PCE decreased to 0.89% ($+2.1 \times 10^6$ V/m).

To identify the mechanism for increasing photocurrent in PSCs, the incident photon-to-current conversion efficiency (IPCE) characteristic of the devices was

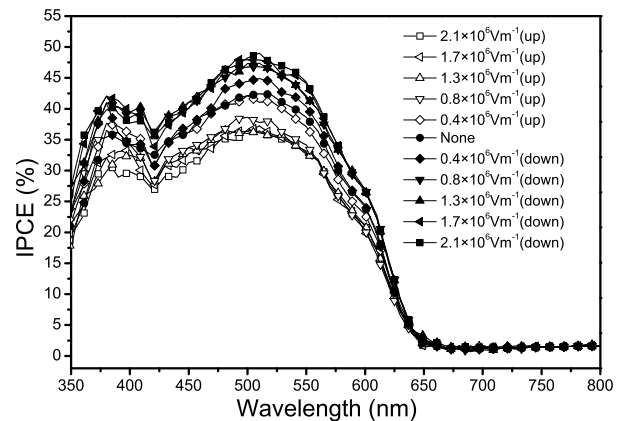


FIG. 4. The IPCE spectra of PSCs with different vertical electric fields.

measured^{17,24}. IPCE depends on both the absorption of light and the collection of charges. Then, the collection of charges depends on the exciton diffusion, separation and carries transport. Figure 4 shows IPCE as a function of spectra within the range of 350-800 nm corresponding to the different treatment with vertical EEFs. The treatment of the EEFs did not change the absorption spectra domain compared to the general PSC, but it can increase or reduce IPCE. For the down EEFs applied from 0.4×10^6 V/m to 2.1×10^6 V/m, the maximum of IPCE increased from 44% to 49%, respectively, of which the amplification is obviously compared with the maximum IPCE (42%) when there is not EEF treatment. On the contrary, for the up EEF of 2.1×10^6 V/m, the maximum of IPCE decreased to 36%. As a conclusion, the treatment of the down EEF has changed the internal molecular order structure of the active layer and the interface structure between active layer and PEDOT:PSS layer, therefore can afford a friendly environment for carrier transport. The active materials of P3HT and PCBM

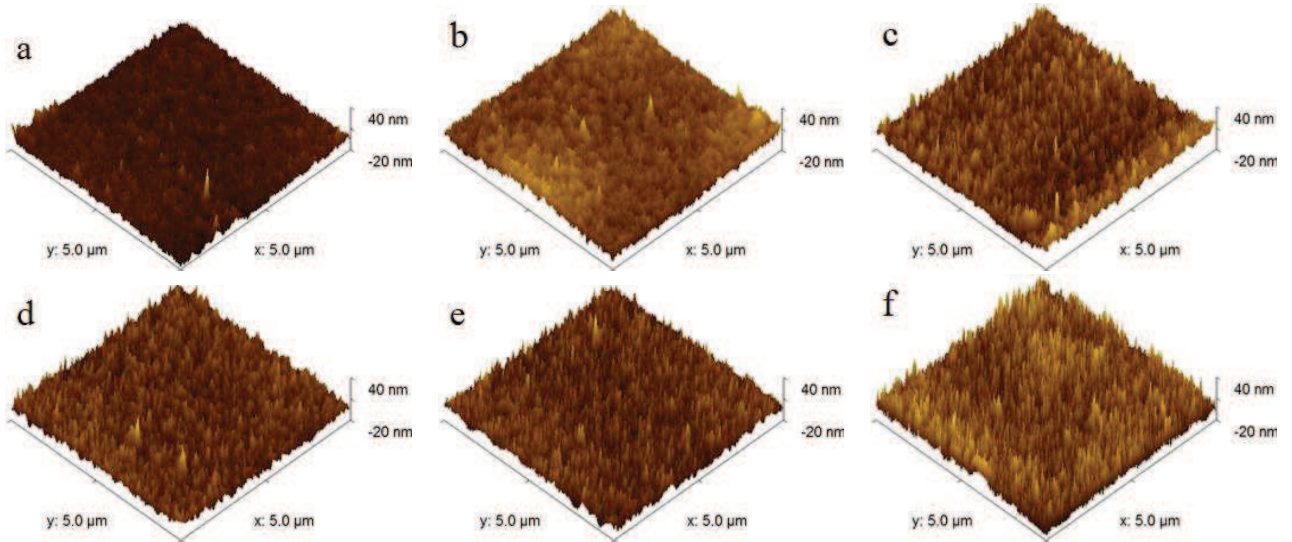


FIG. 5. AFM height images of the surface of P3HT:PCBM thin films (a) with no electric field treatment, and applied with the vertical down electric field for (b) 0.4×10^6 V/m, (c) 0.8×10^6 V/m, (d) 1.3×10^6 V/m, (e) 1.7×10^6 V/m, (f) 2.1×10^6 V/m.

TABLE II. The capacitance value of ITO/PEDOT:PSS/P3HT:PCBM/ITO before and after different vertical electric field treatments.

External electric field (Vm^{-1})	C-before (nF)	C-after (nF)
2.1×10^6 V/m (down)	0.025	0.028
1.7×10^6 V/m (down)	0.023	0.026
1.3×10^6 V/m (down)	0.030	0.021
0.8×10^6 V/m (down)	0.027	0.028
0.4×10^6 V/m (down)	0.030	0.033
0 V/m	0.023	0.024
0.4×10^6 V/m (up)	0.032	0.032
0.8×10^6 V/m (up)	0.024	0.019
1.3×10^6 V/m (up)	0.024	0.020
1.7×10^6 V/m (up)	0.027	0.025
2.1×10^6 V/m (up)	0.027	0.023

are polar molecules. Using a semi-empirical method^{25–27}, we calculated and obtained that the dipole moments of a single molecule of P3HT and PCBM are 0.148D and 4.18D, respectively. In order to know the molecular polarization, the electric capacity of the active layer after adding electric field and annealing process is evaluated. In the annealing process of the active layer, the given electric field is sustained from 110°C to room temperature to ensure the molecules can be controlled by the EEF in the process of crystallization. Table II lists the changes of the electric capacity between the condition with and without an applied EEF. Without EEF, the distribution of the molecules of P3HT and PCBM in the active layer is random and the formed bulk heterojunction is maybe uneven on the macro level. In the case

of the treatment with the applied EEF, for the polar active materials, especially for the strong polar PCBM, a strong polarization in the field direction can take place to make the bulk heterojunction be uniform and ordering. Because of the interaction between the polar active layer and the hole transport material PEDOT:PSS, the applied up EEF reduces the electric capacity value, but the down EEF increases the electric capacity value except one cell (1.3×10^6 V/m). This indicates that the applied EEFs do induce the molecular distribution to be ordering and improve the carrier transport environment in the solar cell.

The morphology of the thin film surface is a key factor for bulk heterojunction in PSCs. Generally, thermal annealing and solvent annealing are popular and effective method to control the morphology^{28–31}. In order to understand the treatment effect on the active layer under the applied electric field during the thermal annealing, the atomic force microscopy (AFM) in tapping mode is used to probe the surface morphology of the active layer.

Figure 5 displays AFM image of the surface morphology of the film built with P3HT:PCBM under different down EEF treatments. As a visual inspection effect, the morphologies of the films show a property that the surfaces change from smooth and bland one to rough and tussocky shapes along with the enhancement of the EEF. It indicates that the applied electric field induces the polar molecules, especially for PCBM, to erect forming a spicules surface during the annealing process. The measured surface roughness (root-mean-square values) of the films with and without electric field (down direction) are as follow,

1.35 nm (0 V/m), 1.45 nm (0.4×10^6 V/m), 1.70 nm (0.8×10^6 V/m), 1.86 nm (1.3×10^6 V/m), 2.00 nm (1.7×10^6 V/m), 2.99 nm (2.1×10^6 V/m).

Just like the visual scene, as the EEF increased, the

film becomes rougher to a certain extent which can provide more contact areas with the up Al electrode and lead to a lower series resistor. And hence the larger short-circuit current density J_{sc} in the PSCs. Therefore, this is also an important factor of which PCE and IPCE of PSCs made in this study improve under EEF.

4. CONCLUSION

In conclusion, the influence factor of the electrode geometry on the photovoltaic performance of PSCs is discussed. Under the identical electrode areas and manufacturing conditions, the electrode geometry shows a significant impact on J_{sc} , FF, and PCE; however, it hardly affects V_{oc} . By analyzing the formation process of the electric field in the electrode, we infer that angular electrodes form uneven electric fields that block the carrier transport and reduce the carrier mobility, even in case of excitons. We expect that this work on the electrode geometry is useful for evaluating the performance of PSCs not only in laboratory studies but also in commercial applications.

ACKNOWLEDGEMENT

This work is supported by the National Natural Science Foundation of China under grant No. 11074066.

- ¹F. C. Krebs, J. Alstrup, H. Spanggaard, K. Larsen, and E. Kold, *Solar energy materials and solar cells* **83**, 293 (2004).
- ²F. C. Krebs, M. Jørgensen, K. Norrman, O. Hagemann, J. Alstrup, T. D. Nielsen, J. Fyenbo, K. Larsen, and J. Kristensen, *Solar Energy Materials and Solar Cells* **93**, 422 (2009).
- ³R. Søndergaard, M. Hösel, D. Angmo, T. T. Larsen-Olsen, and F. C. Krebs, *Materials Today* **15**, 36 (2012).
- ⁴F. C. Krebs, S. A. Gevorgyan, and J. Alstrup, *Journal of Materials Chemistry* **19**, 5442 (2009).
- ⁵G. Li, R. Zhu, and Y. Yang, *Nature Photonics* **6**, 153 (2012).
- ⁶Y. Liang, Z. Xu, J. Xia, S.-T. Tsai, Y. Wu, G. Li, C. Ray, and L. Yu, *Advanced Materials* **22**, E135 (2010).
- ⁷C. H. Peters, I. Sachs-Quintana, W. R. Mateker, T. Heumueller, J. Rivnay, R. Noriega, Z. M. Beiley, E. T. Hoke, A. Salleo, and M. D. McGehee, *Advanced Materials* **24**, 663 (2012).
- ⁸L.-M. Chen, Z. Hong, G. Li, and Y. Yang, *Advanced Materials* **21**, 1434 (2009).
- ⁹G. Dennler, M. C. Scharber, and C. J. Brabec, *Advanced Materials* **21**, 1323 (2009).
- ¹⁰G. Li, V. Shrotriya, J. Huang, Y. Yao, T. Moriarty, K. Emery, and Y. Yang, *Nature materials* **4**, 864 (2005).
- ¹¹V. Dyakonov, *Applied Physics A* **79**, 21 (2004).
- ¹²G. Li, V. Shrotriya, Y. Yao, and Y. Yang, *Journal of Applied Physics* **98**, 043704 (2005).
- ¹³G. Li, Y. Yao, H. Yang, V. Shrotriya, G. Yang, and Y. Yang, *Advanced Functional Materials* **17**, 1636 (2007).
- ¹⁴J. K. Lee, W. L. Ma, C. J. Brabec, J. Yuen, J. S. Moon, J. Y. Kim, K. Lee, G. C. Bazan, and A. J. Heeger, *Journal of the American Chemical Society* **130**, 3619 (2008).
- ¹⁵J. Y. Kim, S. Noh, J. Kwak, and C. Lee, *Journal of Nanoscience and Nanotechnology* **13**, 3360 (2013).
- ¹⁶J. Liu, H. Choi, J. Y. Kim, C. Bailey, M. Durstock, and L. Dai, *Advanced Materials* **24**, 538 (2012).
- ¹⁷A. J. Pearson, T. Wang, R. A. Jones, D. G. Lidzey, P. A. Staniec, P. E. Hopkinson, and A. M. Donald, *Macromolecules* **45**, 1499 (2012).
- ¹⁸C. Kästner, D. K. Susarova, R. Jadhav, C. Ulbricht, D. A. Egbe, S. Rathgeber, P. A. Troshin, and H. Hoppe, *Journal of Materials Chemistry* **22**, 15987 (2012).
- ¹⁹H. Tang, G. Lu, L. Li, J. Li, Y. Wang, and X. Yang, *Journal of Materials Chemistry* **20**, 683 (2010).
- ²⁰G. Sharma, V. Singh Choudhary, and M. Roy, *Solar energy materials and solar cells* **91**, 275 (2007).
- ²¹Y. Li, Y. Hou, Y. Wang, Z. Feng, B. Feng, L. Qin, and F. Teng, *Synthetic metals* **158**, 190 (2008).
- ²²S.-Y. Ma, Y.-M. Shen, P.-C. Yang, C.-S. Chen, and C.-F. Lin, *Organic Electronics* **13**, 297 (2012).
- ²³B. P. Devi, S. Thiyagu, and Z. Pei, *Thin Solid Films* **529**, 54 (2013).
- ²⁴H. Bai, Q. Shi, and X. Zhan, *Organic Optoelectronics* , 407 (2013).
- ²⁵R. C. Chiechi, R. W. Havenith, J. C. Hummelen, L. Koster, and M. A. Loi, *Materials Today* **16**, 281 (2013).
- ²⁶R. K. Bouwer, G.-J. A. Wetzelaer, P. W. Blom, and J. C. Hummelen, *Journal of Materials Chemistry* **22**, 1242 (2012).
- ²⁷G. Volonakis, L. Tsetseris, and S. Logothetidis, *Organic Electronics* **14**, 1242 (2013).
- ²⁸Z. Liang, Q. Zhang, O. Wiranwetchayan, J. Xi, Z. Yang, K. Park, C. Li, and G. Cao, *Advanced Functional Materials* **22**, 2194 (2012).
- ²⁹O. Awartani, B. I. Lemanski, H. W. Ro, L. J. Richter, D. M. DeLongchamp, and B. T. O'Connor, *Advanced Energy Materials* **3**, 399 (2012).
- ³⁰C. R. McNeill, *Energy & Environmental Science* **5**, 5653 (2012).
- ³¹F. Padinger, R. S. Rittberger, and N. S. Sariciftci, *Advanced Functional Materials* **13**, 85 (2003).